Marine Geology 417 (2019) 105988

Contents lists available at ScienceDirect

Marine Geology

journal homepage: www.elsevier.com/locate/margo

Morphological changes in a cuspate sandy beach under persistent high-energy swells: Reñaca Beach (Chile)

R. Agredano[a,b,c,*], R. Cienfuegos[a,c,i], P Catalán[c,d,e], E. Mignot[f], P. Bonneton[g], N. Bonneton[g], C. Martínez[c,h]

[a] Departamento de Ingeniería Hidráulica y Ambiental, Pontificia Universidad Católica de Chile, Vicuña Mackenna 4860, Macul, Santiago, Chile
[b] Centro de Innovación de Ingeniería Aplicada - CIIA, Departamento de Obras Civiles, Facultad de Ciencias de la Ingeniería, Universidad Católica del Maule, Av. San Miguel 3605, Talca, Chile
[c] Centro de Investigación para la Gestión Integrada del Riesgo de Desastres, CONICYT/FONDAP/1511007, Santiago, Chile
[d] Departamento de Obras Civiles, Universidad Técnica Federico Santa María, Avenida España 1680, Valparaíso, Chile
[e] Centro Científico Tecnológico de Valparaíso-CCTVal, Universidad Técnica Federico Santa María, Valparaíso, Chile
[f] LMFA, INSA de Lyon, Université de Lyon, France
[g] UMR EPOC, Université de Bordeaux/CNRS, Talence 33615, France
[h] Instituto de Geografía, Pontificia Universidad Católica de Chile, Vicuña Mackenna 4860, Macul, Santiago, Chile
[i] Marine Energy and Innovation Center (MERIC), Santiago, Chile

ARTICLE INFO

Editor: Prof Edward Anthony

Keywords:
Swash excursion
Wave Steepness
Cusps
Energetic waves

ABSTRACT

The present work proposes a morphological evolution model for sandy cuspate beaches, which depends on two parameters, swash excursion (S) and offshore wave steepness (H_0/L_0). The model was derived from observations of morphology and wave climate at Reñaca Beach in central Chile, comprising in-situ instrumentation, topographic surveys, wave modeling, and optical imagery. It was found that wave steepness alone was unable to explain the morphological changes observed on the beach. Rather, results indicate that swash excursion is better to distinguish between erosive and accretionary events, with swash excursion exceeding 29.5 m for more than 12 h being indicative of erosive events. While morphological changes are led by S, wave steepness correlates with the erosive potential of waves, especially when H_0/L_0 is greater than 0.017. Although derived for a specific beach under a limited range of conditions, this work adds to the understanding of the dynamic behavior of beaches exposed to persistent high-energy swells.

1. Introduction

Sandy beaches may exhibit a highly variable swash zone morphology, influenced by environmental factors acting at different spatial and temporal scales (Larson and C. Kraus, 1995). Despite the available morphodynamic knowledge and models (Dean et al., 1973; Short, 1999; Wright et al., 1979), the understanding of beach dynamics due to natural conditions is not complete.

In the alongshore direction, rhythmic features, termed as beach cusps, are often observed in intermediate to reflective beaches (Wright and Short, 1984). Beach cusp occurrence has not only been reported in sandy beaches but in a wide range of beach environments (Benavente et al., 2011; Masselink and Pattiaratchi, 1998; Nolan et al., 1999; Poate et al., 2013). They are characterized by depressed zones, also known as embayments, which alternate with elevated zones, also known as horns. Although they are ubiquitous forms, there is no consensus regarding the mechanisms explaining their formation. Previous studies have shown that the evolution of beach cusps, growth and decay, was linked to accretionary and erosive events (Almar et al., 2008; Vousdoukas, 2012), but more research is needed to better characterize beach cusp morphodynamics in sandy beaches in terms of their horn and embayment evolution, specially under persistent high-energy swell conditions (Costas et al., 2005; Short and Wright, 1981; Short, 1996; Wright et al., 1979).

In the past decades, several studies have attempted to identify beach states and their link with hydro- and morphodynamic processes. Dimensionless fall velocity, Ω (Dean et al., 1973), has been one of the most used parameters to relate the three-dimensional beach

* Corresponding author at: Av. San Miguel 3605, Talca, Chile.
E-mail addresses: ragredano@uc.cl (R. Agredano), racienfu@ing.puc.cl (R. Cienfuegos), patricio.catalan@usm.cl (P. Catalán), emmanuel.mignot@insa-lyon.fr (E. Mignot), philippe.bonneton@u-bordeaux.fr (P. Bonneton), natalie.bonneton@enseirb-matmeca.fr (N. Bonneton), camartinezr@uc.cl (C. Martínez).

https://doi.org/10.1016/j.margeo.2019.105988
Received 10 June 2018; Received in revised form 15 July 2019; Accepted 15 July 2019
Available online 09 August 2019
0025-3227/

Fig. 1. Study site location. Reñaca Beach in the Valparaíso Region, Chile. Left-upper panel: Valparaíso bay and site location. Right-upper panel: Reñaca Beach study site and location of the ADCP (green triangle) and the video camera for swash excursion analysis (red dot). The area is located in the distal zone of the Valparaíso inlet (red box in the upper-right image) and covers 350 m of the total length of the beach. Bottom image: photograph of the beach study site.

morphology response to wave conditions. Dimensionless fall velocity relates sediment and wave characteristics and was explored by Wright and Short (1984) to distinguish beach morphodynamic states; reflective states when Ω is less than 1; intermediate states for $1 < \Omega < 6$; and dissipative states if Ω is greater than 6. However, since this parameter does not account for tidal range, some limitations in its use have been reported in the literature (Jackson et al., 2005; Masselink and Pattiaratchi, 2001; Vousdoukas et al., 2012).

The distinction between accretion and erosion of beach profiles has been widely associated to thresholds in wave steepness parameter, H_0/L_0 (King, 1972; Komar, 1998; Masselink et al., 2010; Poate et al., 2013, 2014; Sherman, 1991). While Komar (1998) reported the value of $H_0/L_0 = 0.01$ as the limit between accretion (< 0.01) and erosion (> 0.01), King (1972), in field studies, reported wave steepness threshold values ranging from 0.017, for shingle beaches, to 0.011, for fine sand beaches. Other studies have documented thresholds of 0.01

for fine-gravel (Masselink et al., 2010) and 0.007 for coarse-gravel beaches (Sherman, 1991).

Thresholds for the evolution of cuspate beaches have also been established in terms of H_0/L_0, associated to accretionary and erosive swash regimes. Poate et al. (2014) analyzed gravel beaches and found values of $H_0/L_0 < 0.003$ for erosive swash (embayment deepening); values between 0.003 and 0.01 for accretionary swash (horn accretion); values between 0.01 and 0.03 for accretionary swash and smoothing (cusp removal); and values over 0.03 are representative of strong erosion and the disappearance of the cusp system.

Thus, swash dynamics appears to be one of the controlling processes of beach cusp evolution. Masselink and Pattiaratchi (1998) proposed the parameter $\epsilon(S/\lambda)^2$ to characterize the cusp morphodynamics, where ϵ is a parameter that quantifies the difference in the beachface gradient between the cusp horns and embayments, S is the horizontal swash excursion, and λ is the cusp spacing. S is also considered important for beach cusp formation in the self-organization theory of Werner and Fink (1993) and Coco (2003). Masselink and Pattiaratchi (1998) distinguished among three types of morphological responses associated to the swash excursion over the beachface: horn erosion, cusp maintenance, and embayment infilling (or accretion). These authors did not consider other morphological responses such as horn accretion, embayment erosion, or horn and embayment erosion acting together, probably because they were not present during their field observations.

In summary, previous studies support the use of swash excursion measurements to differentiate cuspate beach regimes in combination with the wave steepness. Moreover, the available literature shows that cuspate beach morphodynamics has mostly been investigated in low wave energy microtidal sandy beaches (Coco, 2003; Coco et al., 2004; Masselink et al., 1997, 2004), low-medium energy gravel beaches (Masselink et al., 2010; Poate et al., 2014), and under high energy wave conditions (Masselink et al., 2004; Poate et al., 2013), where swash excursion accounts as an essential parameter controlling morphological changes and cusp evolution. The latter motivates the present research where an attempt to characterize morphological states and beach cusp evolution under persistent high-energy swells in a microtidal sandy beach is undertaken, combining the horizontal swash excursion (S) and the wave steepness (H_0/L_0) parameters. We focus on the characterization of the urban cuspate beach, Reñaca, located in central Chile, which is exposed to shore-normal persistent high-energy south-westerly swells from the Pacific Ocean. Reñaca is a medium-coarse sandy beach, thus the present study complements previous analysis.

In this work we start by describing the study area and then present the methods used for topographic surveys, wave characterization and analysis, and the horizontal swash excursion estimations. The observed morphological states are described next and classified in terms of thresholds in the swash excursion parameter and the wave steepness, followed by a discussion of the results, their relevance and limitations.

2. Study area

Reñaca Beach is located in the Valparaíso Region, (33°S) on the coast of central Chile (Fig. 1). It is a 1200 m long urban beach oriented approximately north to south, exposed to persistent high-energy swells from the Pacific Ocean. The climate is Mediterranean and highly seasonal where the predominant SW winds reach velocities of 4.5 m/s, making it effective for eolian sand transport (Castro and Brignardello, 1997). Statistical analysis of deep-water wave data between 1990 and 2015 (reanalysis data from the Institut Français de Recherche pour l'Exploitation de la Mer - IFREMER) (Ardhuin et al., 2010; Rascle and Ardhuin, 2013) shows that the deepwater wave conditions in Valparaíso Bay are characterized by mean annual significant wave height $H_0 = 1.8$ m (Fig. 2), a mean annual peak wave period $T_p = 11.2$ s, and a mean annual wave direction of 230° (WSW). Records from the Valparaíso tide gauge (Latitude −33.02730833° ; Longitude −71.6259388°), the closest to the study area, show that the tidal range is between 0.26 m and 1.73 m, which allows to classify Reñaca as a microtidal beach (< 2 m Davies, 1972). Intertidal beach profiles measured in 2015 indicate an average intertidal slope of $\beta = 0.1$ and a median grain size of $D_{50} = 0.425$ mm, classified as medium-coarse sand in accordance to the Udden-Wentworth grade scale (Blott and Pye, 2001). Also evident from the observations performed is the presence of rhythmic beach cusp features, like those reported in other nearby beaches in central Chile by Del Canto and Paskoff (1983), Martínez (2007), and Martínez and Salinas (2009). The mean annual dimensionless fall velocity (Wright and Short, 1984) is $\Omega = 2.2$ and the mean annual surf similarity parameter value (Battjes, 1974; Iribarren and Nogales, 1949) is $\xi_b = 1.04$ (both parameters are calculated with breaking wave conditions). These parameters indicate that Reñaca beach can be classified as an intermediate to reflective beach.

3. Materials and methods

3.1. Field campaigns

Wave forcing, swash excursion, and topographic measurements were simultaneously collected during a field campaign between April 1st and April 19th, 2014 (called FC1), with detailed topographic surveys conducted every 1 to 3 days (see Table 1). Topographic surveying was conducted over a longer period in 2015, from the 28th of January to the 29th of June and from the 4th of August to the 10th of August (identified as FC2 in Table 2), on a weekly to bi-weekly basis with 3 to 17 days of separation between consecutive surveys.

The FC1 deployment included (i) a video monitoring system for swash excursion estimation, (ii) topo-bathymetric measurements, and (iii) an ADCP deployment for calibrating deep water wave data with shallow water measurements. For FC2, only video and topographic surveys were collected.

The different methodologies utilized for swash detection, topo-bathymetric surveys, nearshore wave conditions assessment, and the morphological beach state characterization are described in the following subsections.

3.2. Video monitoring and swash detection

The video monitoring system consisted of an IP camera with 2 MegaPixel resolution (Vivotek IP7161), installed in a building in front of the beach (altitude 50 m above msl; see Fig. 1) recording 15-minute videos every half hour during daylight.

13 poles spaced every 2 m were installed in a cross-shore line on the intertidal beachface to provide a geo-referenced grid for rectifying images to the physical space and produce estimations for the swash excursion (Fig. 3.C). Thus, video imagery in combination with topographic data and the geo-referenced cross-shore array of poles were used to get swash excursion measurements.

Swash data were obtained from diagrams derived from the optical data, also known as timestacks (Fig. 3.D). Rectification matrices for the swash excursion detection, were calibrated using direct DGPS measurements on the line of vertical poles installed in the cross-shore profile during FC1 (Fig. 3.C). Both, UTM coordinates and pixel positions for poles in the images were known (Fig. 3.A), but intermediate points and positions beyond the limits of the pole array had to be inter/extrapolated. An inter/extrapolation method using a 2nd order polynomial fit was found to be the most convenient adjustment between pixels and UTM coordinates (see Fig. 3.B).

A semiautomatic swash detection algorithm was applied to 15 min timestack images, based on the Otsu's thresholding method (Otsu, 1979), and results were converted to time series of water level elevations measured relative to the mean sea level (see Fig. 3D). Different cross-shore beach profiles were covered during the FC1 experiment, and rectification matrices were calibrated for each case.

Swash data obtained in FC1 and FC2, from the video monitoring

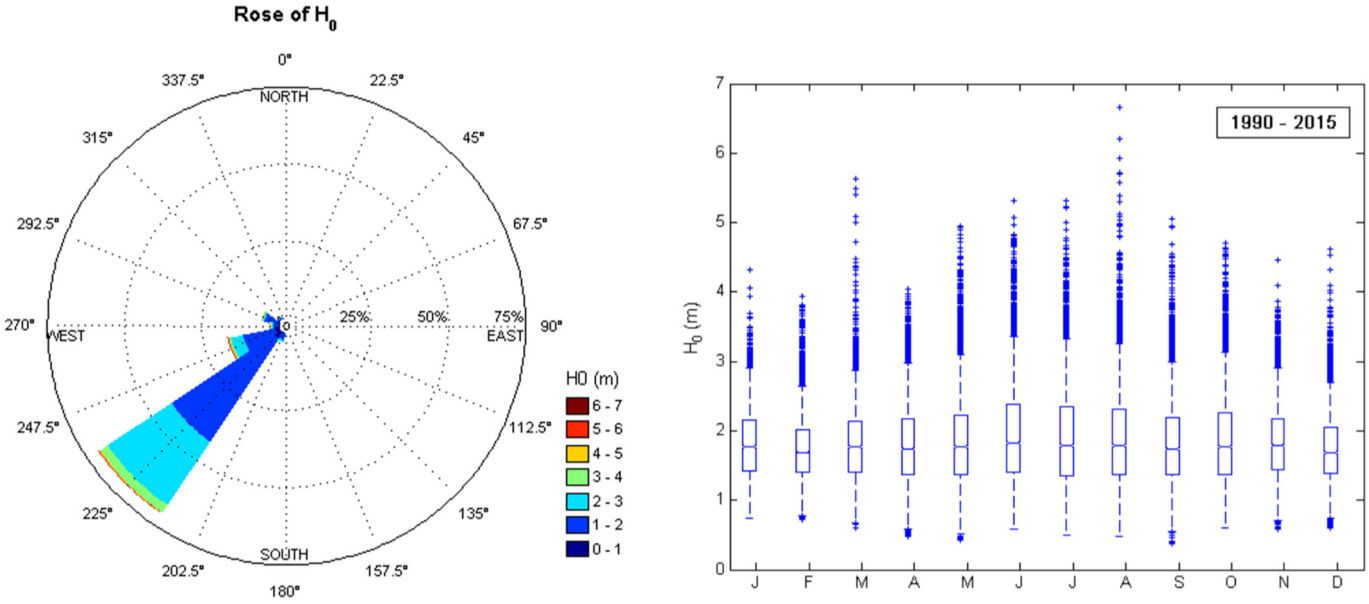

Fig. 2. Historical wave statistics from reanalysis data of the Institut Français de Recherche pour l'Exploitation de la Mer - IFREMER (−33 lat; −72.5 long) between 1990 and 2015. Left panel: Wave rose. Right panel: Monthly evolution of significant wave heights.

system, were used to i) calibrate the Stockdon et al. (2006)'s formula for incident swash, and, ii) compute swash excursion from wave data when video observations were not available for FC2. Vertical swash excursion data from the original formula ($S_{Stockdon}$) and vertical swash excursion data calibrated for Reñaca Beach($S_{Reñaca}$) are used and compared in subsection 4.1. It is worth noting that, for the analysis presented later, the horizontal swash excursion, denoted by S, was used instead of vertical swash excursion. The conversion was done simply dividing vertical swash excursion by the beach slope.

3.3. Topo-bathymetric measurements

Topographic measurements were conducted using a Trimble PPK (Post Processing Kinematic) DGPS logging continuously, once per day during low tide. The relative precision of the topographic surveys depends on the precision of the PPK DGPS (± 0.03 m).

A grid with 1.5 –5 m spacing, depending on the cusp size, is used to ensure that the three-dimensionality of the terrain is captured (Lopes et al., 2013). The topographic surveys were rotated into a local coordinate system for visualization purposes and then interpolated into a uniform 1.5 × 1.5 m grid using the scale-controlled interpolation method (Plant et al., 2002). Various parameters were extracted from the topographic measurements, such as volume changes between consecutive surveys and beachface slopes (β). The volume variation was obtained by the difference of the overlapping beach area of consecutive topographical surveys, and the rest of the parameters were extracted through direct measurement from the interpolated surface.

The RMS of the intertidal topographic elevations was also computed to test cusp changes (Vousdoukas, 2012), showing cusp definition or a flattening state when RMS increases or decreases, respectively. The RMS elevation is represented by:

$$RMS = \sqrt{\frac{1}{l}\int_0^l [Z(\chi) - \bar{Z}]^2 d\chi} \quad (1)$$

where Z is the vertical elevation for a given χ position in the alongshore profile, $\bar{Z}$ is the mean elevation in the alongshore profile, and l is the length of the entire alongshore profile.

During FC1 a single-beam bathymetric survey was performed in the area fronting Reñaca Beach from a depth of 2 to 25 m. This bathymetric data was combined with nautical charts from SHOA (2009) for propagating deep water wave data into the nearshore area in front of Reñaca beach as explained in subsection 3.4.

3.4. Wave data

Modeled offshore wave data for central Chile is available from the open-access reanalysis produced by the Institut Français de Recherche pour l'Exploitation de la Mer (IFREMER) (Ardhuin et al., 2010; Gibson et al., 1996; Rascle and Ardhuin, 2013). Outputs from the reanalysis were obtained every three hours from a model node located at latitude −33° and longitude −72.5° (offshore data from node 33°; 89 km away from the Reñaca Beach). Significant wave height H_0, mean wave period T_z, peak wave period T_p, mean wave direction θ_0, and peak wave direction θ_p were obtained from this dataset.

A Teledyne Sentinel series ADCP (Acoustic Doppler Current Profiler; 1200 Hz) was moored in front of the beach at 12 m depth and 320 m offshore during FC1 (Fig. 1, right-upper panel). Thus, nearshore wave conditions and tidal range were measured every thirty minutes during

Table 1
Field campaign measurements in April 2014 (FC1). Gray boxes indicate the days when each measurement or experiment are deployed.

Year	2014																	
Month	4																	
Day	1	2	3	4	5	6	7	8	9	10	11	12	13	14	15	16	17	18	19
Video Monitoring System																		
Topography																		
Pole experiment																		
ADCP (H_s, T_p, θ)																		

Table 2
Same as Table 1 during field campaigns in 2015(FC2).

Year	2015																		
Month	1	2			3				4					5				8	
Day	28	14	21	26	6	15	20	27	1	10	17	24	29	5	8	16	24	29	4	10
Video Monitoring System																			
Topography																			

the entire observation period. The ADCP data ($H_{s,ADCP}$ and $T_{p,ADCP}$) and the detailed bathymetric survey of the area allow the calibration of deep water reanalysis data using the method proposed by Mínguez et al. (2011) and Tomás (2009). It consists of a parametric calibration to correct the medium and medium-high regime of waves. First, $H_{0,IFREMER}$ and $T_{p,IFREMER}$ need to be propagated from IFREMER node 33 to the ADCP position through spectral wave propagation using the SWAN Model (Simulating WAves Nearshore) (Booij et al., 1999). Then, $H_{0,IFREMER(propagated)}$ and $T_{p,IFREMER(propagated)}$ are compared to $H_{s,ADCP}$ and $T_{p,ADCP}$. Using this procedure, the calibration parameters of the potential function, a and b in Eq. (2) and c and d in Eq. (3), are estimated by an iterative process until convergence between the reanalysis node data and the ADCP observations is achieved, with the final results of $H_{0,calibrated}$ and $T_{p,calibrated}$.

$$H_{0,calibrated} = a*H_{0,IFREMER}{}^{b} \quad (2)$$

$$T_{p,calibrated} = c*T_{p,IFREMER}{}^{d} \quad (3)$$

The hydrodynamic parameters, $H_{0,calibrated}$ and $T_{p,calibrated}$ are necessary to calibrate the Stockdon et al. (2006)'s formula and compute wave steepness for Reñaca. In the remaining of the paper these variables are denoted as H_0 and T_p, for simplicity.

3.5. Determination of morphological beach states

The classification presented here follows Masselink and Pattiaratchi

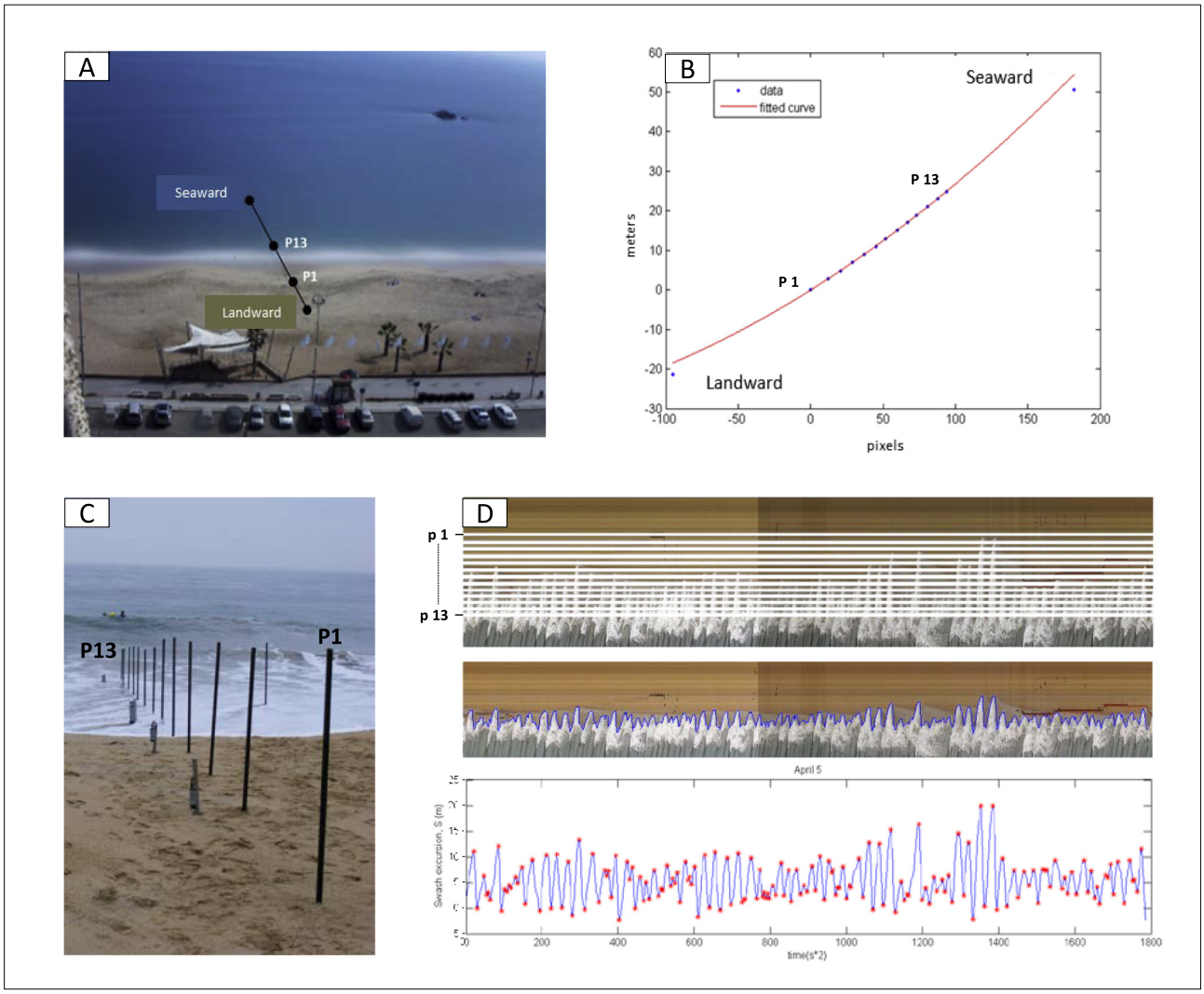

Fig. 3. Pole experiment for extracting swash excursion in combination with the video monitoring system. (A) Pole positions on the beach. (B) mapping of pixel positions of the poles into the physical coordinates, and the 2nd order polynomial fit to get the extreme positions of the profile (Landward and Seaward). (C) Picture of poles installed on the beach. (D) From top to bottom, individual timestack between every pole (from P1 to P13), detection of the swash line (blue line in the middle panel of D), and swash excursion time series rectified. Example for April 5, 2014 (FC1).

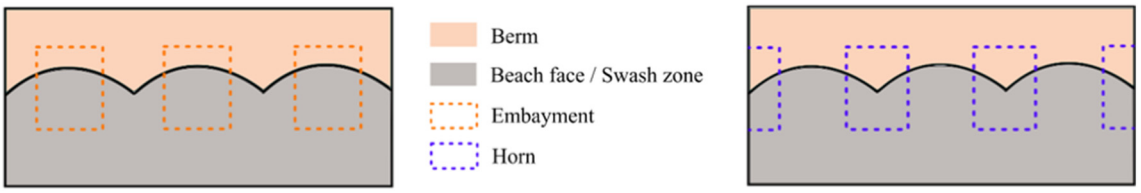

Fig. 4. Sketch of embayment and horn positions to classify each morphological state. In both panels the upper orange part represents the sub-aerial berm and the bottom grey part represents the swash zone. On the left, embayments are framed and, on the right, horns are framed.

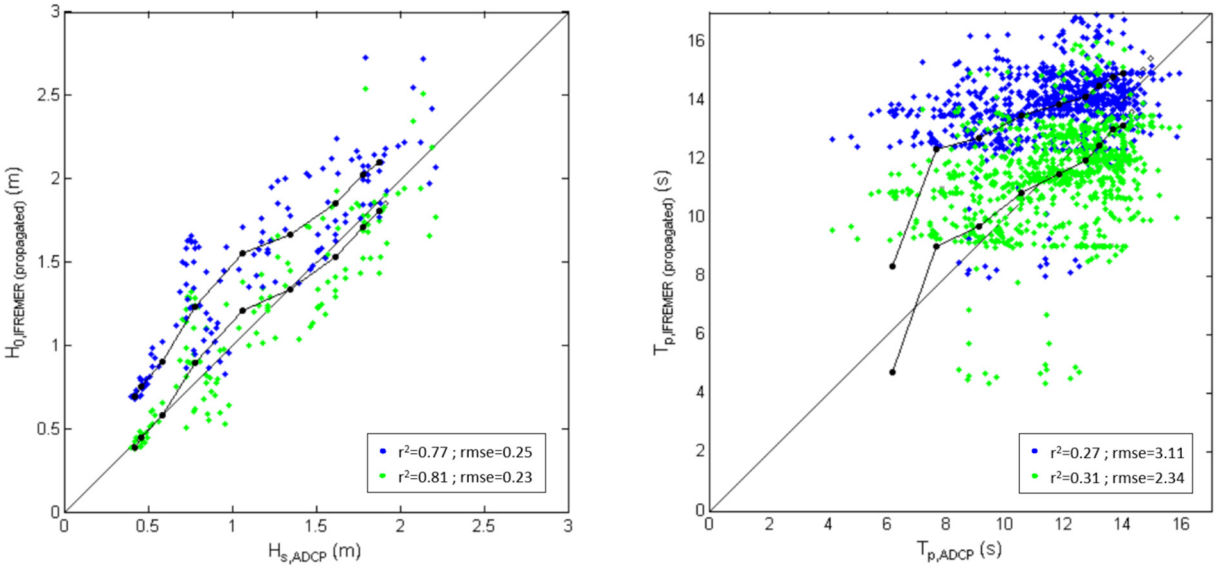

Fig. 5. Scatter plot of propagated IFREMER data to the ADCP position versus the data measured by the ADCP. Left panel is for wave height and right panel is for peak period. In both panels, for *y* axis, blue dots represent the original IFREMER data propagated to the ADCP position, while green dots represent IFREMER data first calibrated and then propagated to the ADCP position. $H_{s,ADCP}$ and $T_{p,ADCP}$ represent data measured with ADCP. Black lines represent the quantiles of wave height and peak period respectively.

(1998) and Poate et al. (2014). Masselink and Pattiaratchi (1998) consider horn erosion, cusp maintenance, and embayment infilling (accretion) as a function of swash excursion values, while Poate et al. (2014) consider embayment deepening (erosion), horn deposit (accretion), smoothing, and cusp reset as a function of changes in the wave steepness. These two classifications are combined for Reñaca beach following two criteria. The first one is to identify the position of the change, horn or embayment, according to the areas in Fig. 4. And the second one refers to the type of change, erosion or accretion, in terms of net sediment volume. Based on these criteria, the following beach morphological states were determined:

- Horn accretion (HA)
- Embayment accretion (EA)
- Horn erosion (HE)
- Embayment erosion (EE)
- Complete erosion or reset (RE) (horn and embayment erosion)

If the largest observed elevation change (accretion or erosion) between surveys occur in horns or embayments (Fig. 4), these cases are classified respectively as horn or embayment accretion/erosion.

For the purpose of linking hydrodynamic parameters (H_0 and T_p) and adequately assess a discriminator of morphological changes, swash excursion and wave steepness are calculated as the average of the highest one-third (33%) of parameter values that occur in a given period as, $S_{1/3} = \frac{1}{n/3}\sum_{i=1}^{i=n/3} S_i$ and $(H_0/L_0)_{1/3} = \frac{1}{n/3}\sum_{i=1}^{i=n/3}(H_0/L_0)_i$, (i = 1,2,...), where n is the number of data between two consecutive topographic surveys ordered from highest to lowest value. Other parameter explored for this purpose is the dimensionless fall velocity (Ω) (Dean et al., 1973) that incorporates breaking waves and sediment characteristics:

$$\Omega = H_b/(w_s{*}T) \quad (4)$$

where H_b is the wave breaking height; w_s is the sediment fall velocity (computed as in Garcia (2008)), and T is the mean wave period computed from T_p as in Pecher and Kofoed (2017). The dimensionless fall velocity also leads to the highest one-third statistics between consecutive surveys, $\Omega_{1/3} = \frac{1}{n/3}\sum_{i=1}^{i=n/3}\Omega_i$, (i = 1,2,...). H_b is computed with SWAN assuming a depth to height ratio of 0.78 according to Battjes and Janssen (1978). Three bathymetric and computational grid resolutions are implemented, 200 × 200, 50 × 50 and 10 × 10 m, and the propagation model is set to stationary mode, breaking and whitecapping are activated and jonswasp spectral shape is used. The onset of wave breaking is obtained when the fraction of energy dissipation due to depth induced wave breaking is non-zero.

4. Results

4.1. Wave data and swash excursion

Using field observations and the methodologies described in the previous section, wave height ($H_{0,IFREMER}$) and peak wave period ($T_{p,IFREMER}$) in deep waters were calibrated using $H_{s,ADCP}$ and $T_{p,ADCP}$, where Eq. (2) and (3) become:

$$H_0 = H_{0,calibrated} = 0.625{*}H_{0,IFREMER}^{1.21} \quad (5)$$

$$T_p = T_{p,calibrated} = 0.1{*}T_{p,IFREMER}^{1.81} \quad (6)$$

Figure (5) shows ADCP data ($H_{s,ADCP}$ and $T_{p,ADCP}$) versus IFREMER

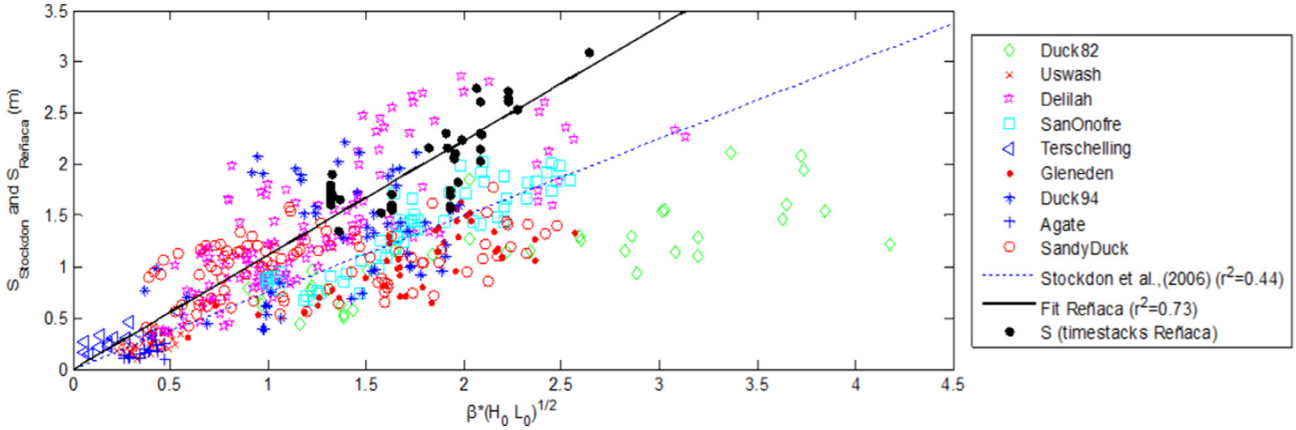

Fig. 6. Original data and regression for Stockdon et al. (2006)'s relation, and recalibrated relation using data from Reñaca Beach. Regressions are forced through the origin to avoid non-physical intercepts. Vertical axis represents vertical swash excursions.

data, first calibrated (H_0 and T_p) and then propagated to the ADCP position ($H_{0,IFREMER(propagated)}$ and $T_{p,IFREMER(propagated)}$), where correlations are also presented.

Based on the proposed methodology, for the entire surveyed period, the mean significant wave height is $H_0 = 1.84$ m, the mean peak wave period $T_p = 11.4$ s, and the mean direction $\theta = 225°$, which are thus in agreement with historical data statistics from 1990 to 2015 (see Section 2). In Figure (7) and (8), time series for the different parameters considered in the study are summarized.

With calibrated wave conditions and the swash excursion data, the empirical formula proposed by Stockdon et al. (2006) is calibrated in order to extrapolate swash excursion data beyond the days where video images are available. The formula calibrated for Reñaca Beach is the following:

$$S_{Reñaca} = 1.117\beta(H_0 L_0)^{1/2} \quad (7)$$

with a correlation of $r^2 = 0.73$ (Figure (6)).

4.2. Morphological responses

In Table 3, morphological responses for each period between surveys were classified. Most periods were clearly identified with one morphological change, except periods 27/03–01/04 and 29/04–05/05 where the combination of two morphological changes was shown. Examples of each morphological state, are presented in Figs. 9 to 13.

The two *HA* periods reported were characterized by an accumulation of sediments mainly in horn areas (see Fig. 4), i.e., when maximum elevation changes occur at the center of the horns by accretion (example in Fig. 9). This is also evident in the increase of the RMS elevation values (Fig. 9, bottom-right) where the cusp system becomes more defined.

The seven *EA* periods reported were characterized by accumulation of sediments where the maximum elevation changes were confined in the embayments (example in Fig. 10). As a consequence of the sediment deposition in the embayments, the lower part of the beach changes toward a more planar state with lower cusp definition, where the cross-shore RMS elevation values decrease significantly on the beachface (Fig. 10, bottom-right).

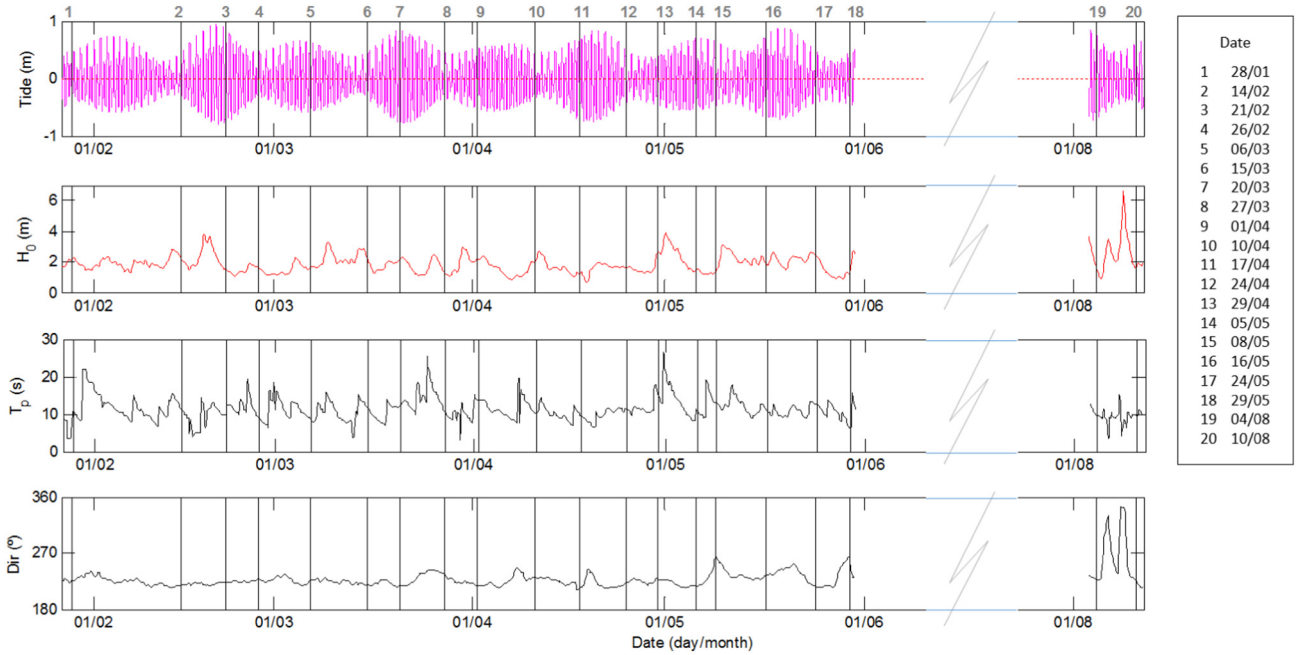

Fig. 7. Tidal record and wave conditions time series for Reñaca beach in 2015. From top to bottom: tidal level recorded by the Valparaíso tide gauge, deep-water significant wave height H_0, peak wave period T_p, and mean wave direction *Dir*. The vertical lines indicate the topographical surveys.

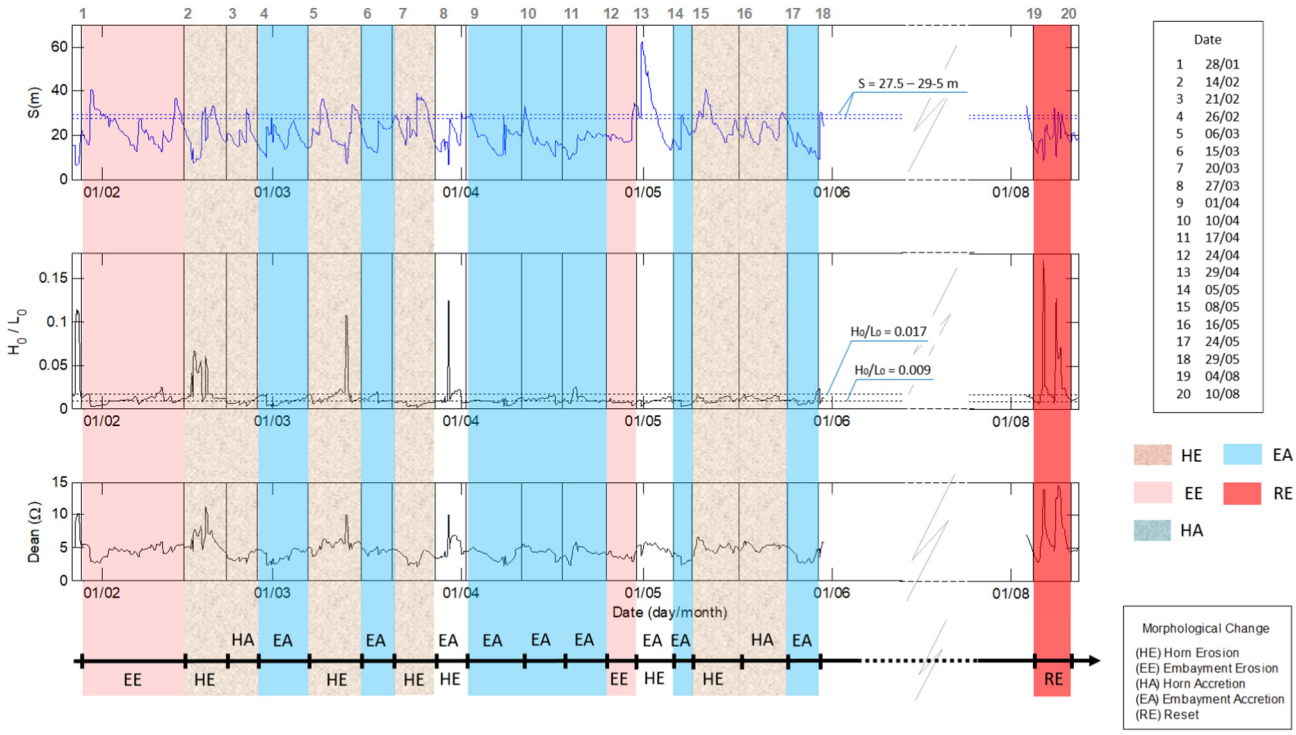

Fig. 8. Time series for Reñaca Beach in 2015, where vertical lines represent the moments of topographical surveys. From top to bottom: horizontal swash excursion *S*, wave steepness (H_0/L_0), dimensionless fall velocity (Ω), and morphological changes between consecutive measurements. Morphological changes are identified in coloured shaded areas. Horizontal lines in *S* and H_0/L_0 represent thresholds explained in results section.

Table 3
Summary of hydrodynamic parameters and morphological states between consecutive measurements. The measurement periods are between 28/01/2015–29/05/2015 and 04/08/2015–10/08/2015.

Date of topography		$S_{1/3}$ (m)	$S_{máx}$ (m)	$H_0/L_{0,1/3}$	$H_0/L_{0,máx}$	$\Omega_{1/3}$	Volumes (m³)		Tide	Morphological evolution
1st data	2nd data						Erosion	Accretion		
28/01/2015	14/02/2015	31,18	40,9	0,0149	0,0251	2,6623	3520	1547	NT-ST-NT	EE
14/02/2015	21/02/2015	29,70	33,5	0,0463	0,0664	3,2416	5320	792	NT-ST	HE
21/02/2015	26/02/2015	24,90	32,0	0,0098	0,0128	2,2234	140	4863	ST-NT	HA
26/02/2015	06/03/2015	23,76	28,3	0,0139	0,0181	2,3568	265	3178	NT-ST	EA
06/03/2015	15/03/2015	31,84	36,5	0,0303	0,1080	3,0956	2395	898	ST-NT	HE
15/03/2015	20/03/2015	24,44	26,5	0,0149	0,0197	2,4118	42	3167	NT-ST	EA
20/03/2015	27/03/2015	34,44	39,1	0,0080	0,0085	2,6453	4726	669	ST-NT	HE
27/03/2015	01/04/2015	26,50	30,2	0,0270	0,1255	3,1395	808	883	NT-ST	EA & HE
01/04/2015	10/04/2015	25,54	29,6	0,0103	0,0126	2,3850	250	2024	ST-NT	EA
10/04/2015	17/04/2015	24,07	33,2	0,0134	0,0155	2,7946	405	2179	NT-ST	EA
17/04/2015	24/04/2015	20,84	21,8	0,0161	0,0251	2,5978	440	2330	ST-NT	EA
24/04/2015	29/04/2015	25,64	34,5	0,0087	0,0115	2,1558	2000	330	NT-ST	EE
29/04/2015	05/05/2015	48,07	62,6	0,0120	0,0145	2,8634	2460	2331	ST-NT	HE & EA
05/05/2015	08/05/2015	25,81	29,5	0,0097	0,0102	2,0018	710	1836	ST-NT	EA
08/05/2015	16/05/2015	32,34	41,3	0,0134	0,0151	3,6451	7352	1282	NT-ST	HE
16/05/2015	24/05/2015	27,21	30,3	0,0147	0,0159	3,6218	532	1543	ST-NT	HA
24/05/2015	29/05/2015	22,06	27,3	0,0128	0,0201	2,5714	394	1750	NT-ST	EA
04/08/2015	10/08/2015	26,07	32,9	0,0671	0,1715	2,8851	10819	275	ST-NT	RE

S: horizontal swash excursion; H_0/L_0: wave steepness; Ω: Dean´s number; ST: Spring tide; NT: Neap tide
HA: Horn accretion; EA: embayment accretion; HE: Horn erosion; EE: Embayment erosicn; RE: Complete erosion (Reset)

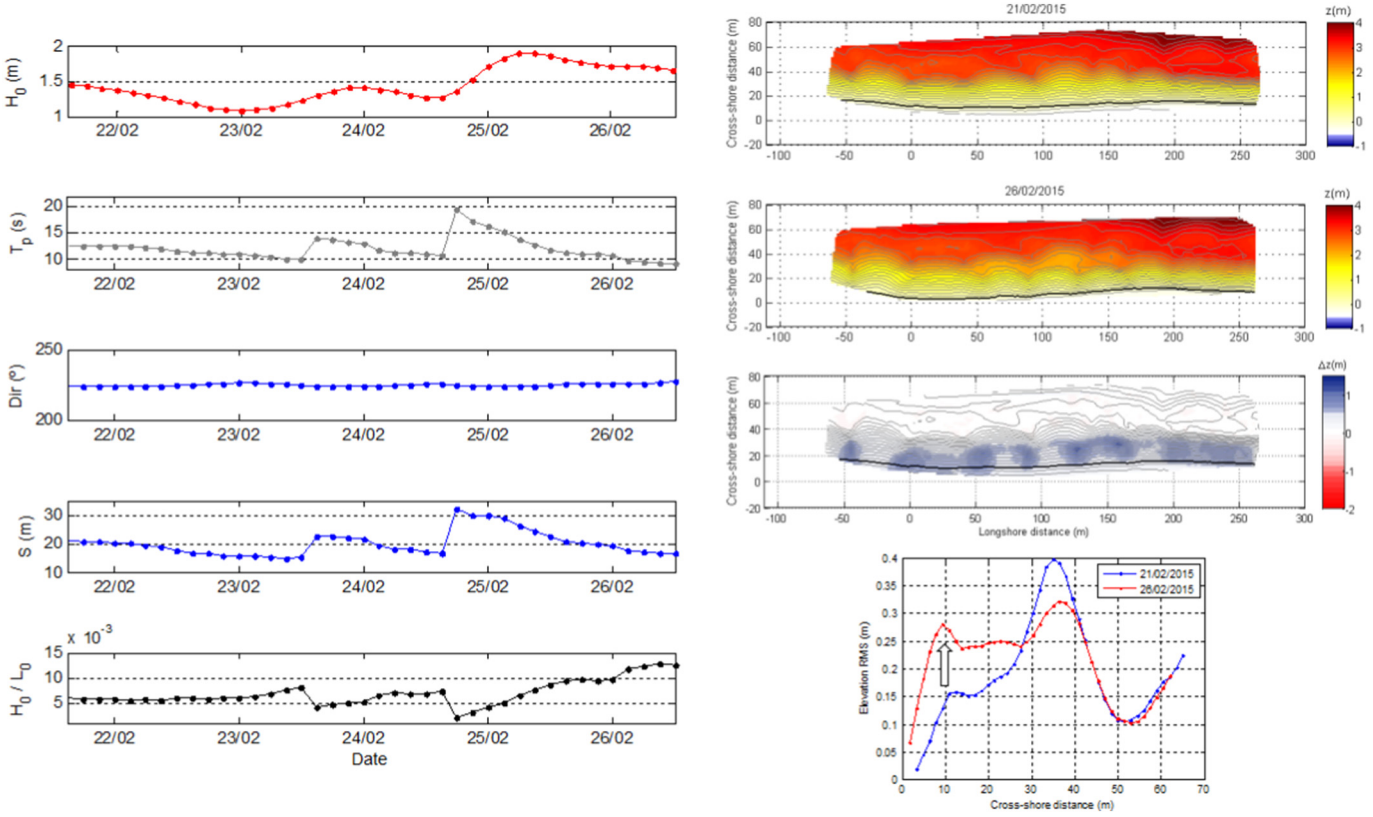

Fig. 9. Example of morphological response of type "horn accretion" between 21/02/2015 and 26/02/2015. Left panel: deep-water significant wave height H_0(m), peak wave period T_p(s), mean wave direction *Dir*, horizontal swash excursion *S*(m) and wave steepness H_0/L_0. Right panel: 3D morphological surface at the beginning and end of period, corresponding difference of bed elevation Δz(m) and cross-shore elevations RMS, for both measurements. Maximum Δz are located in horns and RMS increase from the beginning to the end of period which represent a cusp system more defined.

The four observed *HE* periods were defined by the loss of sediments with the maximum elevation changes confined in horns (example in Fig. 11). The consequence of horn erosion on the beachface is the decrease in the cross-shore RMS elevation values in the zone of wave influence, where the cusp system is smoothed (Fig. 11, bottom-right).

The only two periods of *EE* were characterized by loss of sediments centered in the embayments (example in Fig. 12). Embayment erosion tends to accentuate the cusp system, with greater cross-shore RMS elevation values on the beachface, as shown in Fig. 12 (bottom-right).

The only period of *RE* was a combination of *HE* and *EE* with the consequence of the complete erosion of the beachface (Fig. 13). Only one large erosion event (see Fig. 13) was observed in 2015; it was accompanied with a significant loss of sediments (more than 10,000 m^3), as estimated from consecutive topographic surveys. A beach retreat of nearly 40, equivalent to an area of approximately 4500 m^2, was also observed.

The period in which this event occurred was characterized by a storm with maximum wave height of H_0 = 6.6 m on the 8th of August (Eq. (7)), which was the maximum wave height of the entire dataset (Fig. 2). The wave direction of this storm was North-West (Fig. 7), thus different from the more frequent South-West waves. As a consequence, the cusp system disappeared completely and the beachface was eroded and flattened to an approximate cross-shore distance of 40 m (Fig. 13). The RMS is smaller after the storm, increasing toward land due to the resulting vertical scarp (Fig. 13, bottom-right). It is worth noting that this event was preceded by another storm of lower intensity that removed a volume of sand of approximately 3000 m^3 between 05/08 and 07/08 (Fig. 14.B). The combination of these two events increased the erosive response and caused the retreat of the shoreline and the formation of a beach scarp (Fig. 14, B and C).

The remaining periods are those where two morphological changes appear in the observations, 27/03–01/04 (EA & HE) and 29/04–05/05 (HE & EA) (Table 3). Even when the erosion and accretion occur in these periods, the net volume is close to zero and the beach tends to evolve towards a more planar configuration, filling embayments and eroding horns. The volume change was 808 m^3 for erosion and 883 m^3 for accretion in the first period, and 2460 m ^{3} for erosion and 2331 m^3 for accretion in the second period.

Statistical parameters, $S_{1/3}$ and $(H_0/L_0)_{1/3}$, were calculated for all periods and are presented in Fig. 15.A. All accretion morphological changes occur when $S_{1/3} < 27.5$ m and $(H_0/L_0)_{1/3}$ is between 0.009 and 0.017. For erosion changes (including *RE*) the values of $S_{1/3}$ and $(H_0/L_0)_{1/3}$ are outside the limits where accretion occurs. Moreover, most of the erosion events are observed when $S_{1/3} > 29.5$ m. Only two erosion events, one in *EE* and the *RE* event are observed when $S_{1/3} < 27.5$ m, but those have extreme values of $(H_0/L_0)_{1/3}$, $(H_0/L_0)_{1/3} = 0.0087$ for the *EE* case (less than the limit of 0.009 for accretions) and $(H_0/L_0)_{1/3} = 0.0671$ for the *RE* case (larger than 0.017 limit established for accretions).

It is also important to note that in Fig. 15.A, neither erosion or accretion periods are observed for values of $S_{1/3}$ between $S_{1/3} = 27.5$ m and $S_{1/3} = 29.5$ m, hence these values appear to represent a threshold band to discriminate between accretion and erosion regimes, but no specific behavior can be inferred inside this band.

The following threshold values can be established from the observations conducted in Reñaca Beach:

- $S_{1/3} < 27.5$ m: accretion regimes when $0.009 < (H_0/L_0)_{1/3} < 0.017$
- $S_{1/3} > 29.5$m: erosion regimes (regardless of $(H_0/L_0)_{1/3}$)
- $27.5 < S_{1/3} < 29.5$ m: no data in this interval (threshold band)

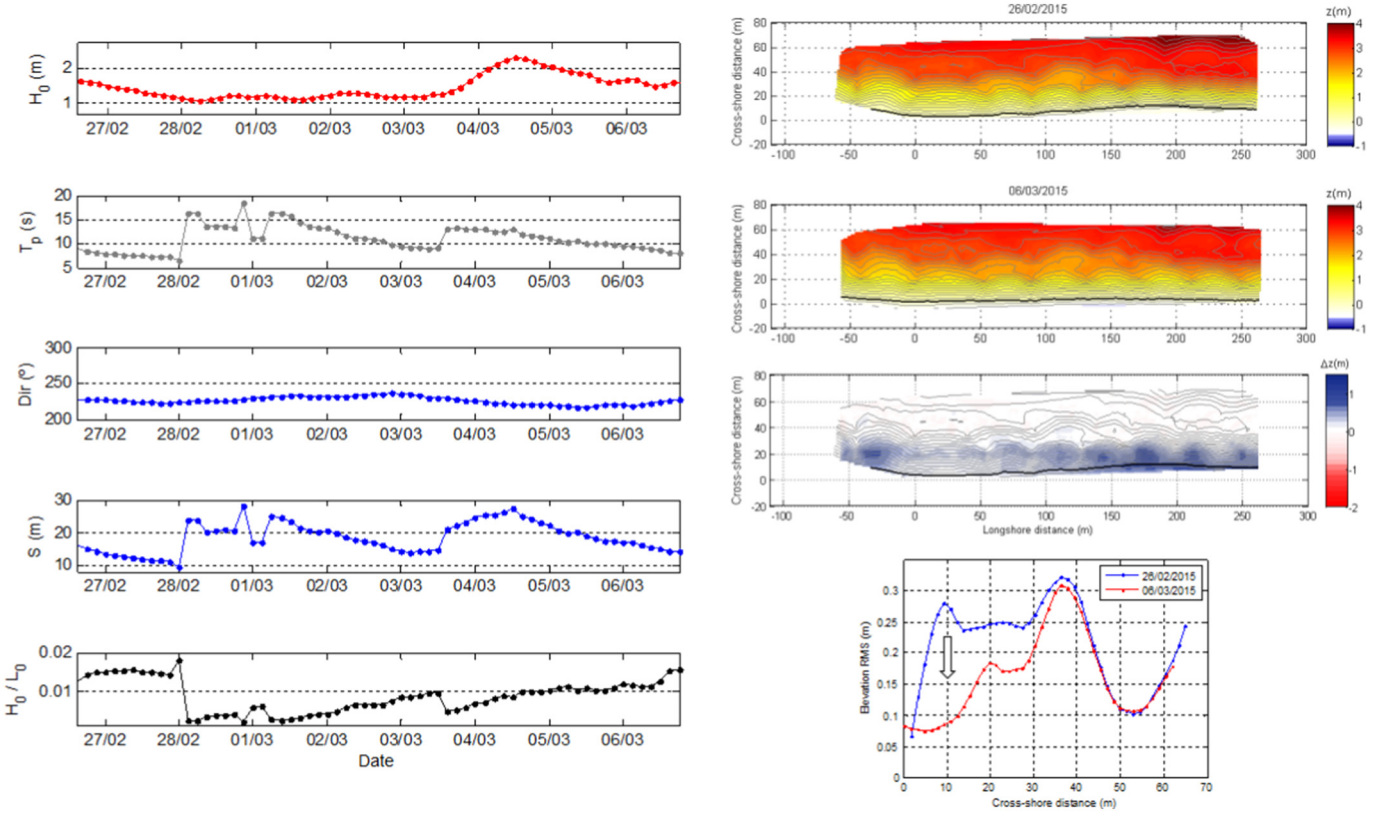

Fig. 10. Same as Fig. 9 but for morphological response of state "embayment accretion" recorded between 26/02/2015 and 06/03/2015. Maximum Δz are located in embayments and RMS decrease from the beginning to the end of period which represent a cusp system less defined (flatter shape).

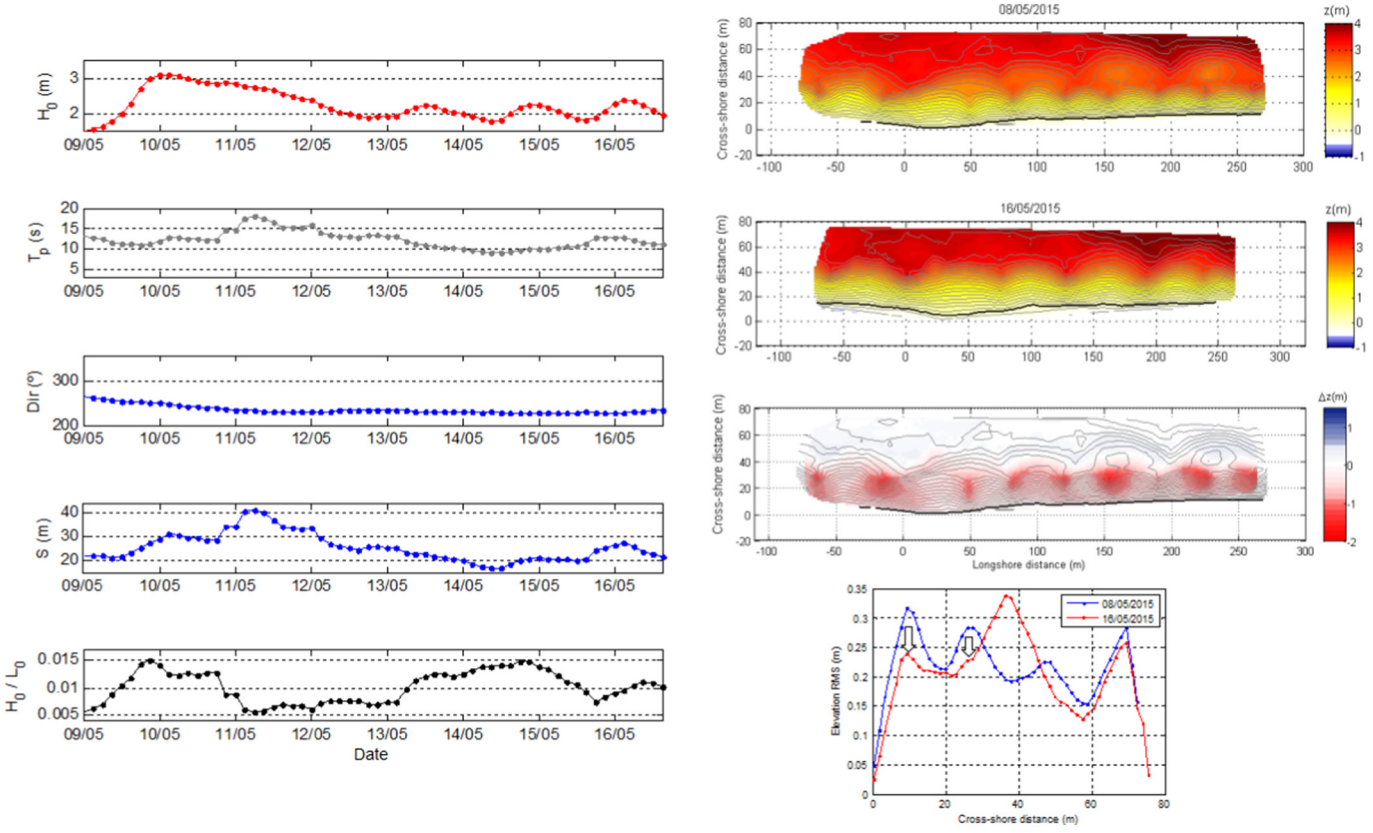

Fig. 11. Same as Fig. 9 but for morphological response of state "horn erosion" recorded between 08/05/2015 and 16/05/2015. Maximum Δz are located in horns and RMS decrease from the beginning to the end of period which represent a cusp system less defined (flatter shape).

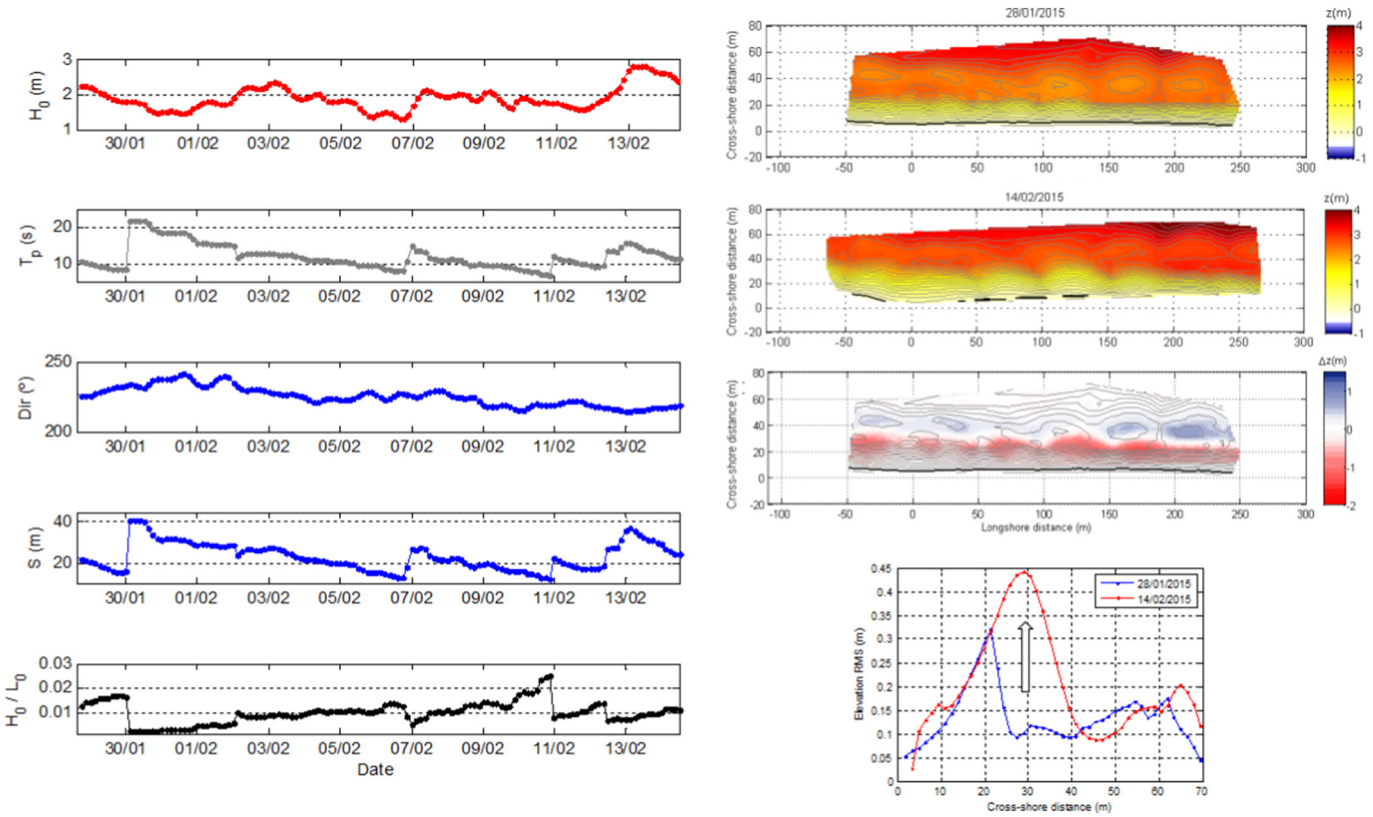

Fig. 12. Same as Fig. 9 but for morphological response of state "embayment erosion" recorded between 28/01/2015 and 14/02/2015. Maximum Δz are located in embayments and RMS increase from the beginning to the end of period which represent a cusp system more defined.

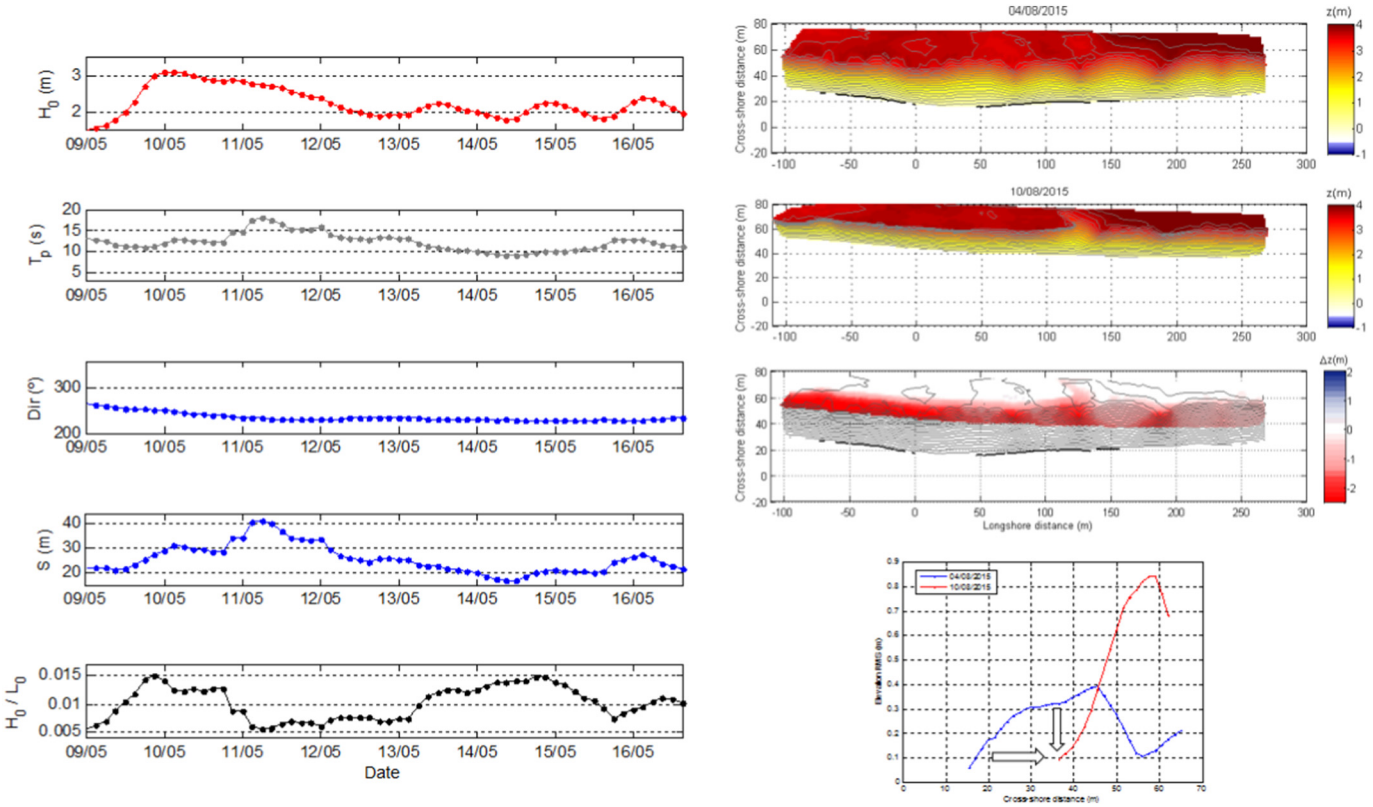

Fig. 13. Same as Fig. 9 but for morphological response of state "complete erosion" of the beachface recorded between 04/08/2015 and 10/08/2015. Maximum Δz are located in all beach. RMS values show that beach turns to a flatter shape with a shoreline retreat more than 20 m.

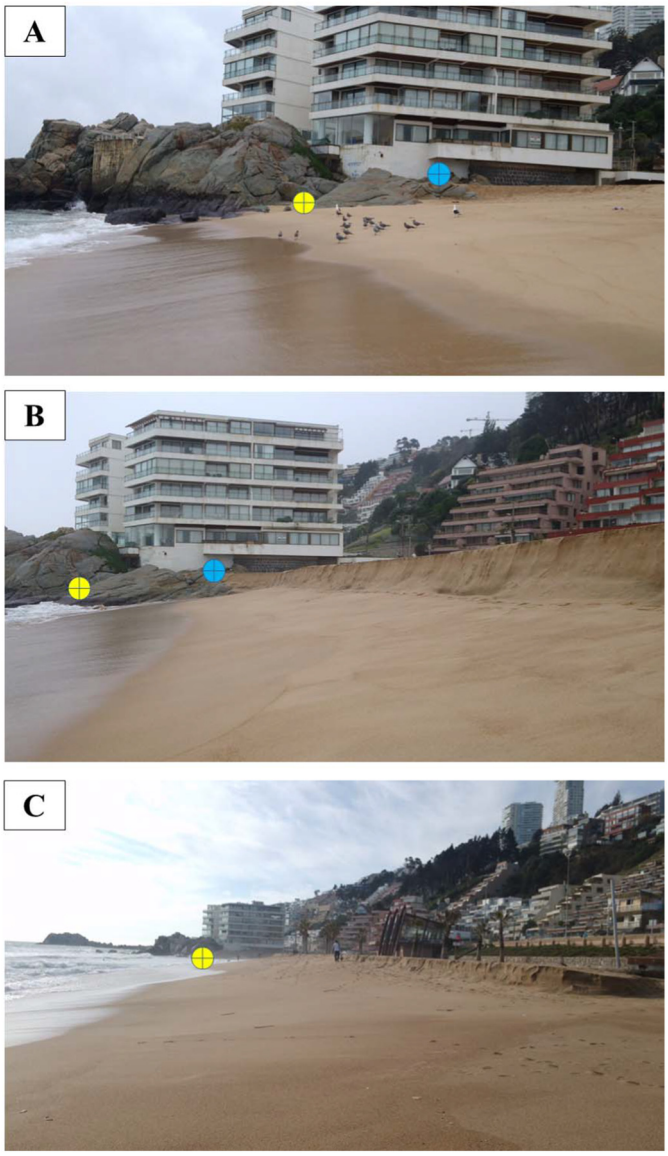

Fig. 14. Images of the morphological change in the northern part of the beach between 04/08/2015 (A), 07/08/2015 (B) and 10/08/2015 (C). The colored circles represent identifiable points in these images that display sand losses.

- $(H_0/L_0)_{1/3} < 0.009$: erosion regimes (regardless of $S_{1/3}$).
- $0.009 < (H_0/L_0)_{1/3} < 0.017$: erosion regimes when $S_{1/3} > 29.5$ m, and accretion regimes when $S_{1/3} < 29.5$ m
- $(H_0/L_0)_{1/3} > 0.017$: erosion regimes (regardless of $S_{1/3}$).

Fig. 15 (A and B) summarizes the threshold for $S_{1/3}$ and $(H_0/L_0)_{1/3}$ that delimit accretionary and erosive regimes between consecutive topographic surveys in Reñaca. Also in Fig. 15.C, the different regimes are presented in the $H_0 - T_p$ space.

4.3. Duration above thresholds

Since the time periods between topographic measurements vary from 3 to 17days(FC2), the time of S and H_0/L_0 above the thresholds established in previous section were also analyzed for each period (Fig. 8), to complement the analysis performed with statistical parameters $S_{1/3}$ and $(H_0/L_0)_{1/3}$. The thresholds for calculating the time above them are $S = 29.5$ m and $H_0/L_0 = 0.017$ (Table 4).

For all accretion periods, S is above 29.5 m for no more than 9 h (Fig. 16.A). In case of H_0/L_0, for HA events H_0/L_0 is always below 0.017, and for EA events H_0/L_0 is over 0.017 for no more than 18 h (Fig. 16.B).

In case of erosion events (*HE* and *EE*), only one case of *EE* (24/04–29/04 in Table 3) have $S_{1/3} < 29.5$ m (also less than 27.5 m), and this case have also the lowest $(H_0/L_0)_{1/3}$ of 0.0087 (below the minimum of 0.009 for all accretions). Even when $S_{1/3} < 29.5$ m, the time over $S = 29.5$ m in this period is 15 h, more than the maximum of 9 h reached in all accretion events (Fig. 16.A). The rest of erosion events exceed $S = 29.5$ m for more than 33 h. In terms of persistence over $H_0/L_0 = 0.017$, three cases exceed 0.017 for more than 27 h and other three cases have no values over 0.017 (Fig. 16.B). These last three cases also have the largest values of S (S_{max} in Table 3).

For *RE* event, even when $S_{1/3} = 26.07$ m (< 29.5 m) for the entire period, the persistence of S over 29.5 m occurs for 12 h(more than maximum of 9 h in accretion events). The particularity here is that $H_0/L_0 = 0.017$ is exceeded for 72 h(Fig. 16.B), the longest time of the entire dataset, which was also when H_0/L_0 reached a higher value of $(H_0/L_0)_{max} = 0.1715$ (Table 3), significantly higher than in all other periods.

Finally, for periods with two morphological changes, in the 27/03–01/04 (EA & HE) period, $S = 29.5$ m were exceeded only for 3 hours, while H_0/L_0 over 0.017 was observed for 36 h, hence doubling the maximum time above threshold of any other accretion period (18 h in 17/04-24-04). For the period between 29/04 and 05/05, the combined HE and EA morphological change was driven by an inverse relationship between parameters, with S exceeding 29.5 m for 72 h(the second longest time of exceed in the entire time series with the maximum S of 62.3 m), but H_0/L_0 was always under 0.017.

These results indicate that swash excursion, in Reñaca Beach, provides better insight than wave steepness (through wave height and peak period) to differentiate between erosive and accretion conditions (as in Bergillos et al. (2016)). Erosion and accretion events are led by S, while H_0/L_0 increases the erosive potential of the waves. Hence, S plays a key role in the cuspate beach dynamics under persistent high-energy swells.

5. Discussion

The prevalence of beach cusp morphology is characteristic of Reñaca, except after extreme events such as the one in August 2015. Although a defined cusp system already existed at the beginning of the measurement period (28/01/2015), to adequately record the morphological changes, wave conditions between two consecutive topographic measurements were considered, instead of those given at the exact moment of the topographic measurements as in Benavente et al. (2011). According to this, the influence of prior wave conditions is fundamental to explain the morphological changes observed. Only two consecutive erosion periods are found in Reñaca (EE between 28/01 and 14/02 followed by HE between 14/02 and 21/02) where S and H_0/L_0 continue over thresholds for 33 and 57 h respectively. $(H_0/L_0)_{max}$ reaches the highest values of the entire dataset (without considering RE) and the second event has more energetic wave conditions. This results in a large amount of sediment moved (5320 m^3 of HE; see Table 3). This effect is also shown between periods 24/04–29/04 (EE) and 29/04–05/05 (HE & EA) with the same behavior of the increase of the energy between the two events. These effects can be considered as the result of storm clustering (consecutive storms). The largest erosion event of August 2015 was also the combination of two storm events (subsection 4.2) with a first erosion of 3000 m^3 and a second extreme erosion of 7819 m^3 (difference between the total erosion of 10, 819 m^3 minus 3000 m^3 in Table 3) where the largest wave height was reported in the historical dataset. The sum of erosion volumes in the period between 28/01–14/02 and 14/02–21/02, 8840 m^3 (3520 m^3 + 5320 m^3 in Table 3), does not differ much from the total erosion in August, 81910819 m^3, and also it is higher than the isolated extreme erosion event of 7819 m^3 in August. This is in agreement with Ferreira (2005), where the erosive effect of consecutive storms with short return periods, can be equivalent to a single large storm event with a longer return period (Ferreira,

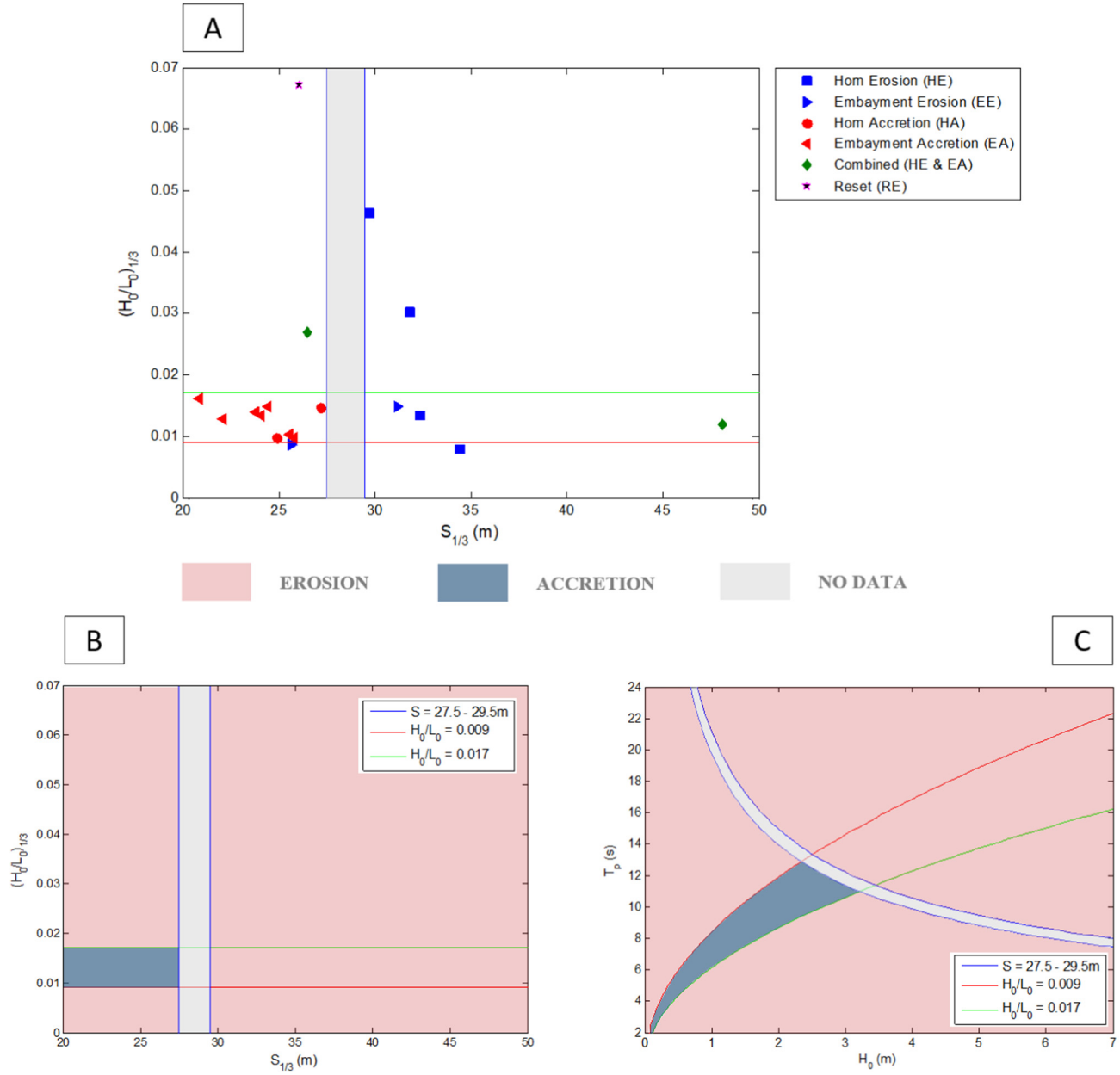

Fig. 15. Morphological beach states of Reñaca Beach as a function of the horizontal swash excursion ($S_{1/3}$) and the wave steepness ($(H_0/L_0)_{1/3}$) in 2015 (A). Solid lines represent thresholds for $S_{1/3}$ =27.5 - 29.5m, $(H_0/L_0)_{1/3}$ =0.009 and $(H_0/L_0)_{1/3}$ =0.017 that differentiate between accretion and erosion events. B and C show the regions where accretion and erosion occurs in terms of $S_{1/3}$ vs $(H_0/L_0)_{1/3}$ (B) and H_0 vs T_p (C).

2005). For all periods with consecutive storm events, the second storm was always more energetic than the first. The inverse situation, reported by Dissanayake et al. (2015) , was not observed in Reñaca beach.

Erosion and accretion were appropriately differentiated, but it was not possible to discriminate between embayments and horns. Other parameters as tidal range and dimensionless fall velocity (Ω) were analyzed to differentiate them (see Table 3). Changes in tidal range (Neap (NT) to Spring (ST) tide and vice versa) show no conclusive trends. Similarly, dimensionless fall velocity did not yield an accurate discrimination, not only between embayment or horn but neither between erosion and accretion (as also Vousdoukas et al. (2012) concluded). There are only two well defined *EE* and one *HA* events in the entire dataset, and this is not enough to conclude about thresholds to differentiate between embayment and horn morphological changes.

Beachface erosion and accretion events have been reported mainly as a function of wave steepness (H_0/L_0), but the results presented demonstrate that this parameter is insufficient or limited to differentiate between these two types of events in Reñaca Beach. In Reñaca all accretion events occur when H_0/L_0 is between 0.009 and 0.017, but erosion events occur with no specific dependence when H_0/L_0 ranges from H_0/L_0 = 0.008 to H_0/L_0 = 0.671 (Table 3). In comparison with other studies, these thresholds do not match prior results (King, 1972; Komar, 1998; Masselink and Pattiaratchi, 2001), hence, other variables should be considered in the analysis to better explain morphological changes in Reñaca. A Principal Component Analysis (PCA) and a Principal Component Regression (PCR) were explored to identify the fundamental variables and combination variables that better explain the cusp morphology (Lopes et al., 2011). The results were consistent with Lopes et al. (2011) where wave height and peak period were the two fundamental variables that explain better the cusp morphology. Since *S* is considered a key parameter in one of the two main theories of cusps dynamics (self-organization theory (Coco et al., 1999; Werner and

Table 4
Surpassed times for swash excursion and wave steepness thresholds.

Date of topography		$t_{S<27.5}$ (h)	$t_{S=27.5-29.5}$ (h)	$t_{S>29.5}$ (h)	$t_{H0/L0<0.009}$ (h)	$t_{H0/L0=0.009-0.017}$ (h)	$t_{H0/L0>0.017}$ (h)	Morphological evolution
1st data	2nd data							
28/01/2015	14/02/2015	291	42	75	162	219	27	EE
14/02/2015	21/02/2015	120	15	33	6	105	57	HE
21/02/2015	26/02/2015	108	3	9	96	24	0	HA
26/02/2015	06/03/2015	195	3	0	99	96	3	EA
06/03/2015	15/03/2015	150	6	54	36	120	54	HE
15/03/2015	20/03/2015	126	0	0	30	87	9	EA
20/03/2015	27/03/2015	96	24	45	165	0	0	HE
27/03/2015	01/04/2015	102	18	3	63	24	36	EA & HE
01/04/2015	10/04/2015	183	27	6	147	69	0	EA
10/04/2015	17/04/2015	153	6	9	36	132	0	EA
17/04/2015	24/04/2015	171	0	0	66	87	18	EA
24/04/2015	29/04/2015	99	3	15	108	9	0	EE
29/04/2015	05/05/2015	60	12	72	63	81	0	HE & EA
05/05/2015	08/05/2015	66	6	3	48	27	0	EA
08/05/2015	16/05/2015	132	15	39	75	111	0	HE
16/05/2015	24/05/2015	156	24	9	6	183	0	HA
24/05/2015	29/05/2015	123	0	0	63	48	12	EA
04/08/2015	10/08/2015	132	6	12	24	54	72	RE

H_0/L_0: wave steepness; S: horizontal swash excursion

HA: Horn accretion; EA: embayment accretion; HE: Horn erosion; EE: Embayment erosion; RE: Complete erosion (Reset)

Fink, 1993)), S was also incorporated as a combination variable in the PCA, PCR and the analysis of erosive and accretion regimes in Reñaca beach. For PCA and PCR, S was found the main combination variable in explain cusp morphology. That supported the inclusion of S in the analysis.

Finally, S data for Reñaca Beach were compared with S data in other beaches with similar mean wave and beach condition (experiments of Duck82 and Duck94 (Stockdon et al., 2006)) to better contextualize this study. Despite the similar characteristics, swash data differ from those in Reñaca Beach(see Fig. 6). Reñaca S data are usually higher than in Duck82 and Duck94 with clearly different trends, specially in Duck82, the most similar to Reñaca of these two Duck experiments. This may be caused by the differences in sediment size (not known in beaches compared) that change swash infiltration values increasing the asymmetry in the swash flow (Masselink and Li, 2001). While deep-water wave height is used in all these experiments, wave measurements from ADCP in Reñaca were used to calibrate deep-water wave heights instead of reverse shoaled to deep-water using linear wave theory as done with the Duck data by Stockdon et al. (2006).

6. Conclusions

The complexity of the hydrodynamic factors involved in beach cusp formation, evolution, and disappearance on beaches dominated by waves, presents great challenges to scientific research, specially regarding the elaboration of predictive models. They involve complex processes in which both the hydrodynamics and the morphology of the beach, influence and co-determine each other. This work presents six months of observations on a sandy beach, where wave conditions are representative of the historical data statistics from 1990 to 2015. The beach was monitored in all possible morphological states and their evolution was surveyed. It was possible to relate the accretion and erosion regimes to thresholds in two parameters, the horizontal swash excursion (S), and the wave steepness (H_0/L_0).

Although the data presented in this work allow to anticipate the morphological changes of the beach, the magnitude of both erosion and accretion is not easily assessed since, in each case, the magnitude of change is also conditioned by the prior state. Also, the differentiation between changes in embayments and horns is not clearly explained with the available data. More extensive monitoring, in terms of both morphological changes and granulometric variations, is required to characterize the amount of eroded or accreted sand.

We conclude that horizontal swash excursion S and wave steepness H_0/L_0 allow us to define thresholds of $S = 29.5$ m and $H_0/L_0 = 0.017$ where erosion events in Reñaca beach occur if they are exceeded for a certain time. For erosion events, S always exceeded 29.5 m for more than 12 h, but H_0/L_0 not always exceeded 0.017. Then, it was found that erosion events are led by S, while H_0/L_0 increases the erosive potential of the waves which are thus able to displace larger volumes of sand.

While these results are important for building predictive models for beach evolution under persistent high-energy swells, additional observations are required to confirm these thresholds in other contexts.

Acknowledgments

Agredano has been supported by the CONICYT National Doctoral Scholarship (project no 21150705) through the Formation of Advanced Human Capital Program of the Chilean Ministry of Education. Agredano and Cienfuegos also thank CONICYT for the FONDECYT 1120878 grant, and Catalán for the FONDECYT 1170415 and PIA/Basal FB0821 (CCTVal) grants. In addition, the authors thank the Centro de Investigación para la Gestión Integrada del Riesgo de Desastres-CIGIDEN (CONICYT/FONDAP 15110017) for financing part of this

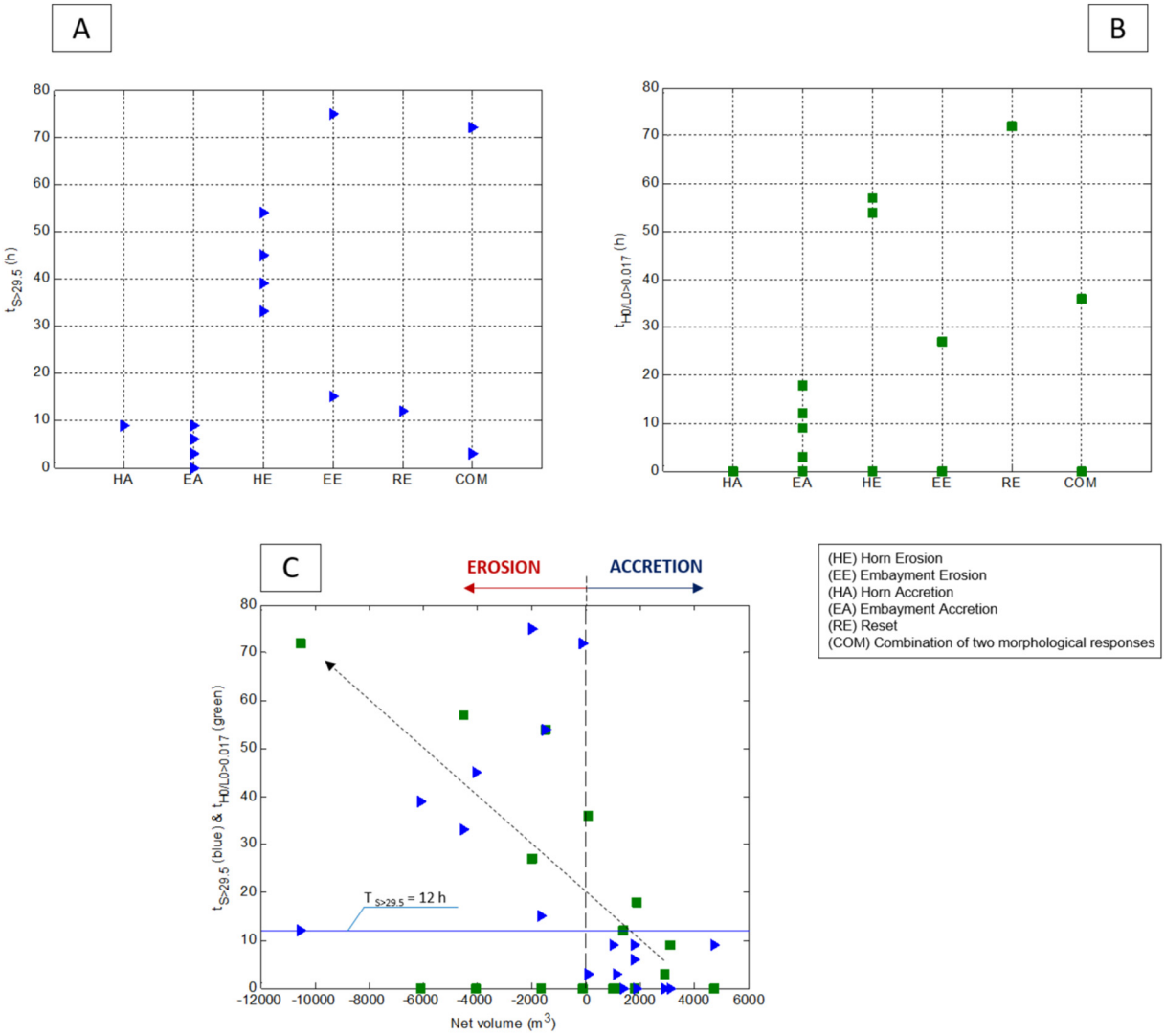

Fig. 16. (A) Time, in hours, that the time series of significant horizontal swash excursion (S in Fig. 8), is exceeded in 29.5m. (B) Time, in hours, that the wave steepness (H_0/L_0 in Fig. 8), exceeds 0.017. (C) Represents the tendency between the time over thresholds, S = 29.5 m and H_0/L_0 = 0.017, and the net volume moved. Horizontal line in (C) represents the minimum time of S over 29.5 m that differentiate between erosion and accretion regimes. For all panels, each value represent one period between two consecutive topographic surveys in the entire 2015 measurement period.

work. We are also greatly indebted to French laboratory UMR-CNRS 5805 EPOC Bordeaux for the collaboration, their instruments and expertise.

References

Almar, R., Coco, G., Bryan, K.R., Huntley, D. a., Short, a. D., Senechal, N., 2008. Video observations of beach cusp morphodynamics. Mar. Geol. 254 (3-4), 216–223. https://doi.org/10.1016/j.margeo.2008.05.008.

Ardhuin, F., Rogers, E., Babanin, A.V., Filipot, J.-F., Magne, R., Roland, A., van der Westhuysen, A., Queffeulou, P., Lefevre, J.-M., Aouf, L., Collard, F., 2010. Semiempirical dissipation source functions for ocean waves. Part I: definition, calibration, and validation. Journal of Physical Oceanography 40 (9), 1917–1941. https://doi.org/10.1175/2010JPO4324.1.

Battjes, J.A., 1974. Surf similarity. 14th Conference on Coastal Engineering. ASCE 466–480.

Battjes, J.A., Janssen, J., 1978. Energy loss and set-up due to breaking of random waves. Coastal Engineering Proceedings 1 (16).

Benavente, J., Harris, D.L., Austin, T.P., 2011. Medium term behavior and evolution of a beach cusps system in a low energy beach, Port Stephens, NSW, Australia . J. Coast. Res. Spec. Issue (64), 170–174.

Bergillos, R.J., Ortega-Sánchez, M., Masselink, G., Losada, M.A., 2016. Morpho-sedimentary dynamics of a micro-tidal mixed sand and gravel beach, Playa Granada, Southern Spain. Mar. Geol. 379, 28–38.

Blott, S.J., Pye, K., 2001. Gradistat: a grain size distribution and statistics package for the analysis of unconsolidated sediments. Earth Surf. Process. Landf. 26 (11), 1237–1248.

Booij, N.R.R.C., Ris, R.C., Holthuijsen, L.H., 1999. A third-generation wave model for coastal regions: 1. Model description and validation. J. Geophys. Res. Oceans 104, 7649–7666.

Castro, C., Brignardello, L.-A., 1997. Geomorfología aplicada a la ordenación territorial de la franja costera entre Concón y Quintay (3 2 O 55 ' s y 33 " 15 ' s)'. Revista de Geografía Norte Grande 125, 113–125.

Coco, G., 2003. Test of self-organization in beach cusp formation. J. Geophys. Res. 108 (C3), 1–11. https://doi.org/10.1029/2002JC001496.

Coco, G., Burnet, T.K., Werner, B., Elgar, S., 2004. The role of tides in beach cusp development. J. Geophys. Res. Oceans 109 (C4).

Coco, G., O'Hare, T.J., Huntley, D. a., 1999. Beach cusps: a comparison of data and theories for their formation. J. Coast. Res. 15 (3), 741–749.

Costas, S., Alejo, I., Vila-Concejo, A., Nombela, M.A., 2005. Persistence of storm-induced morphology on a modal low-energy beach: a case study from nw-iberian peninsula. Mar. Geol. 224 (1-4), 43–56.

Davies, J.L., 1972. Geographical variation in coastal development. Oliver and Boyd.

Dean, R.G., et al., 1973. Heuristic models of sand transport in the surf zone. In: First Australian Conference on Coastal Engineering, 1973: Engineering Dynamics of the Coastal Zone, pp. 215.

Del Canto, S., Paskoff, R., 1983. Características y evolución geomorfológica actual de algunas playas de Chile central, entre Valparaíso y San Antonio (V Región). Revista de Geografía Norte Grande 10, 31–45.

Dissanayake, P., Brown, J., Wisse, P., Karunarathna, H., 2015. Comparison of storm cluster vs isolated event impacts on beach/dune morphodynamics. Estuar. Coast. Shelf Sci. 164, 301–312.

Ferreira, Ó., 2005. Storm groups versus extreme single storms: predicted erosion and management consequences. J. Coast. Res. 221–227.

Garcia, M.H., 2008. Sediment transport and morphodynamics. In: Sedimentation

Engineering: Processes, Measurements, Modeling, and Practice, pp. 21–163.
Gibson, R., Kallberg, P., Uppala, S., 1996. The ECMWF Reanalysis (ERA) Project. ECMWF Newsl., 73 7–17.
Iribarren, C.R., Nogales, C., 1949. Protection des ports. XVIIth International Navigation Congress. PIANC.
Jackson, D., Cooper, J., Del Rio, L., 2005. Geological control of beach morphodynamic state. Mar. Geol. 216 (4), 297–314.
King, C.A.M., 1972. Beaches and Coasts. 113. St Martin Press., pp. 70–85.
Komar, P., 1998. Beach Processes and Sedimentation. Prentice-Hall, Englewood Cliffs, New Jersey.
Larson, M., Kraus, N.C., 1995, aug, aug. Prediction of cross-shore sediment transport at different spatial and temporal scales. Mar. Geol. 126 (1-4), 111–127. https://doi.org/10.1016/0025-3227(95)00068-A.
Lopes, V., Baptista, P., Pais-Barbosa, J., Taveira-Pinto, F., Veloso-Gomes, F., 2013. DGPS based methods to obtain beach cusp dimensions. J. Coast. Res. 65 (sp1), 541–546.
Lopes, V., Pais-Barbosa, J., Taveira-Pinto, F., Veloso-Gomes, F., 2011. Beach cusps: using multivariate data analysis techniques for the identification of important variables and for predicting their spacing. J. Coast. Res. (64), 1106–1110.
Martínez, C., 2007. Shoreline changes in Concón and Algarrobo bays, central Chile, using an adjustment model. Investig. Mar. 35 (2), 99–112. https://doi.org/10.4067/S0717-71782007000200010.
Martínez, C., Salinas, S., 2009. Morfodinámica y evolución reciente de playa Tunquén, Chile central. Revista de Biologia Marina y Oceanografia 44 (1), 203–215. https://doi.org/10.4067/S0718-19572009000100021.
Masselink, G., Hegge, B., Pattiaratchi, C., 1997. Beach cusp morphodynamics. Earth Surf. Process. Landf. 22, 1139–1155. https://doi.org/10.1002/(SICI)1096-9837(199712)22:12<1139::AID-ESP766>3.0.CO;2 -1.
Masselink, G., Li, L., 2001. The role of swash infiltration in determining the beachface gradient: a numerical study. Mar. Geol. 176 (1-4), 139–156.
Masselink, G., Pattiaratchi, C., 2001. Seasonal changes in beach morphology along the sheltered coastline of Perth, Western Australia. Mar. Geol. 172 (3-4), 243–263.
Masselink, G., Pattiaratchi, C.B., 1998. Morphological evolution of beach cusps and associated swash circulation patterns. Mar. Geol. 146 (1-4), 93–113. https://doi.org/10.1016/S0025-3227(97)00129-1.
Masselink, G., Russell, P., Blenkinsopp, C., Turner, I., 2010. Swash zone sediment transport, step dynamics and morphological response on a gravel beach. Marine Geology 274 (1-4), 50–68. https://doi.org/10.1016/j.margeo.2010.03.005.
Masselink, G., Russell, P., Coco, G., Huntley, D., 2004. Test of edge wave forcing during formation of rhythmic beach morphology. J. Geophys. Res. Oceans 109 (C6).
Mínguez, R., Espejo, A., Tomás, A., Méndez, F.J., Losada, I.J., 2011. Directional calibration of wave reanalysis databases using instrumental data. J. Atmos. Oceanic Tech. 28 (11), 1466–1485. https://doi.org/10.1175/JTECH-D-11-00008.1.
Nolan, T., Kirk, R., Shulmeister, J., 1999. Beach cusp morphology on sand and mixed sand and gravel beaches, South Island, New Zealand. Mar. Geol. 157 (3), 185–198. https://doi.org/10.1016/S0025-3227(98)00150-9.
Otsu, N., 1979. A threshold selection method from gray-level histograms. IEEE Trans. Syst. Man Cybern. 9 (1), 62–66.
Pecher, A., Kofoed, J.P., 2017. Handbook of Ocean Wave Energy. Springer.
Plant, N.G., Holland, K.T., Puleo, J. a., 2002. Analysis of the scale of errors in nearshore bathymetric data. Mar. Geol. 191 (1-2), 71–86. https://doi.org/10.1016/S0025-3227(02)00497-8.
Poate, T., Masselink, G., Davidson, M., McCall, R., Russell, P., Turner, I., 2013. High frequency in-situ field measurements of morphological response on a fine gravel beach during energetic wave conditions. Mar. Geol. 342, 1–13. https://doi.org/10.1016/j.margeo.2013.05.009.
Poate, T., Masselink, G., McCall, R., Russell, P., Davidson, M., 2014. Storm-driven cusp behaviour on a high energy gravel beach. J. Coast. Res. Proceeding (70), 645–650. https://doi.org/10.2112/SI70-109.1.
Rascle, N., Ardhuin, F., 2013. A global wave parameter database for geophysical applications. Part 2: model validation with improved source term parameterization. Ocean Modelling 70, 174–188. https://doi.org/10.1016/j.ocemod.2012.12.001.
Sherman, D., 1991. Gravel beaches. Natl Geogr. Res. Explor. 7 (4), 442–452.
SHOA, 2009. Atlas Hidrográfico de Chile. Valparaíso: SHOA. SHOA.
Short, A., Wright, L., 1981. Beach systems of the Sydney region. Aust. Geogr. 15 (1), 8–16.
Short, A.D., 1996. The role of wave height, period, slope, tide range and embaymentisation in beach classifications: a review. Rev. Chil. Hist. Nat. 69, 589–604.
Short, A.D., 1999. Handbook of Beach and Shoreface Morphodynamics. John Wiley. Ltd. Chichester, England.
Stockdon, H.F., Holman, R.A., Howd, P.A., Sallenger, A.H., 2006. Empirical parameterization of setup, swash, and runup. Coast. Eng. 53 (7), 573–588. https://doi.org/10.1016/j.coastaleng.2005.12.005.
Tomás, A., 2009. Calibration methodologies of wave reanalysis data bases (in Spanish). Ph.D. Thesis, Departamento de Ciencias y Técnicas del Agua y del Medio Ambiente 310.
Vousdoukas, M.I., 2012. Erosion/accretion patterns and multiple beach cusp systems on a meso-tidal, steeply-sloping beach. Geomorphology 141-142, 34–46. https://doi.org/10.1016/j.geomorph.2011.12.003.
Vousdoukas, M.I., Almeida, L.P.M., Ferreira, Ó., 2012. Beach erosion and recovery during consecutive storms at a steep-sloping, meso-tidal beach. Earth Surf. Process. Landf. 37 (6), 583–593. https://doi.org/10.1002/esp.2264.
Werner, B.T., Fink, T.M., 1993. Beach cusps as self-organized patterns. Science (New York, N.Y.) 260 (5110), 968–971. https://doi.org/10.1126/science.260.5110.968.
Wright, L., Chappell, J., Thom, B., Bradshaw, M., Cowell, P., 1979. Morphodynamics of reflective and dissipative beach and inshore systems: Southeastern Australia. Mar. Geol. 32, 105–140.
Wright, L., Short, A., 1984. Morphodynamic variability of surf zones and beaches: a synthesis. Mar. Geol. 56 (1-4), 93–118. https://doi.org/10.1016/0025-3227(84)90008-2.